

Interfacing picosecond and nanosecond quantum light pulses

Filip Sośnicki,^{1,*} Michał Mikołajczyk,¹ Ali Golestani,¹ and Michał Karpiński¹

¹*Faculty of Physics, University of Warsaw, Pasteura 5, 02-093 Warszawa, Poland*

(Dated: November 10, 2022)

Light is a key information carrier, enabling worldwide high-speed data transmission through a telecommunication fibre network. This information-carrying capacity can be extended to transmitting quantum information (QI) by encoding it in single photons – flying qubits. However, various QI-processing platforms operate at vastly different timescales. QI-processing units in atomic media, operating within nanosecond to microsecond timescales, and high-speed quantum communication, at picosecond timescales, cannot be efficiently linked due to orders of magnitude mismatch in the timescales or, correspondingly, spectral linewidths. In this work, we develop a large-aperture time lens using complex high-bandwidth electro-optic phase modulation to bridge this gap. We demonstrate coherent, deterministic spectral bandwidth compression of quantum light pulses by more than two orders of magnitude with high efficiency. It will facilitate large-scale hybrid QI-processing by linking the ultrafast and quasi-continuous-wave experimental platforms, which until now, to a large extent, have been developing independently.

Single photons are perfect candidates for transmitting quantum information between different quantum systems [1, 2]. The timescales of such quantum light pulses can vary significantly depending on the platform employed. Single-photon pulse duration is linked to its spectral bandwidth via the time-bandwidth product, which places a lower limit on the spectral bandwidth required to support a pulse of a given duration, via the time-bandwidth product. Two classes of QI-processing platforms can be distinguished when taking the timescale as a criterion. The first one comprises ultrafast systems, where the employed photon durations are on the order of single picoseconds, corresponding to hundreds of GHz of spectral bandwidths [3]. They are based mostly on optical nonlinearities such as three- or four-wave mixing, with the particular example of widely used spontaneous parametric down-conversion (SPDC) photon-pair sources and nonlinear optical gating [4, 5]. Additionally, they can be implemented with a high repetition rate. Thanks to similar spectral bandwidths used in the classical telecommunication, they are also compatible with already existing high-speed telecom fibre networks. The latter class incorporates slower systems with nanosecond-long pulses and MHz up to single GHz-wide spectra. It primarily includes matter-based systems, such as single atoms [6, 7] or their ensembles [8–10]. It also incorporates colour-centres in diamond, solid-state QI processing platforms [11, 12] and optomechanics [13]. Such systems provide quantum memories with long storage time [14–16] and single-photon nonlinearities [17, 18] required to perform optical QI processing, however they are inherently slow. For example, a system with 10 MHz spectral bandwidth is fundamentally limited to operate at most at 100 ns repetition rate. Large-scale QI processing is envisioned to take advan-

tage of all the mentioned systems, creating a hybrid quantum network or a quantum Internet [19, 20]. A challenge arises to connect the two classes of quantum systems efficiently, to combine the QI processing capabilities of the slow systems with the photon generation and efficient communication capabilities, as well as the speed of the fast systems.

A possible solution would be staying within the slow regime, employing mostly matter-based platforms. One could employ known methods to generate spectrally narrow, temporally long photons [12, 21]. However, narrow spectra and long photon pulses limit the overall QI-processing network performance due to low achievable repetition rates. Additionally, such MHz-wide optical pulse spectra are incompatible with telecom components such as wavelength-division multiplexing (WDM). A different approach is directly connecting ultrafast and matter-based systems. However, it would result in spectral filtering of broadband photons, which is inherently lossy and incoherent, again reducing the network performance. For example, reducing the single-photon bandwidth by a factor of N is probabilistic with a success rate of approximately $1/N$. This probability scales exponentially as $(1/N)^M$ with the number M of such interfaces.

Instead, a coherent interface, enabling low-loss shaping of quantum light pulses in time and spectrum, is required to efficiently combine the two classes of quantum devices to form a quantum network operating at a high repetition rate [22, 23]. Such an interface needs to redistribute the energy across the single-photon pulse, simultaneously increasing its duration and narrowing its spectrum. It needs to be realized using phase-only operations, without resorting to filtering or amplification, and with low insertion loss. It requires a combination of pulse propagation in a dispersive medium combined with time-dependent phase modulation.

The phase-only quantum interfaces demonstrated to date allow for spectral manipulations only within the ultrafast regime, i.e. from multi-THz down to tens of GHz spectral widths. Previous works report spectral bandwidth conversion, obtained either by optical three-wave-mixing [22, 24] and cross-phase modulation [25]. Single-photon-level light manipulation using the four-wave-mixing scheme has also been demonstrated [26, 27]. However, the nonlinear approaches suffer from high insertion loss and optical noise due to limited conversion efficiency and the use of a strong pump. The electro-optic approach was the first to demonstrate efficient coherent spectral bandwidth modification of single-photon pulses [23, 28], thanks to its deterministic nature. It has inherent unit conversion efficiency with a limiting factor of only technical losses and allows for easy central wavelength tunability. Additionally, spectral-temporal manipulation of single-photon pulses employing electro-optic phase modulation can be performed in a low-loss, all-fibre platform without the necessity of optical pumping, thus without adding optical noise to the quantum signal [23]. However, up till now, high spectral modification factors, necessary for linking the ultrafast and slow QI processing platforms, have not been realized electro-optically due to limited electro-optic phase modula-

* Filip.Sosnicki@fuw.edu.pl

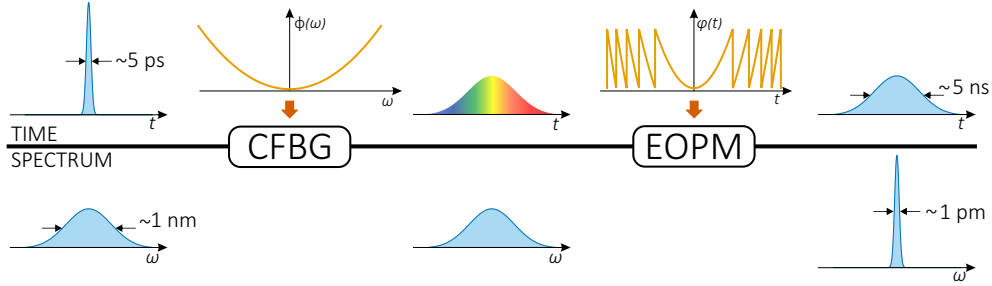


Figure 1. **Conceptual scheme of large-scale spectral bandwidth conversion.** It shows manipulation of the temporal profile (upper part) and spectrum (bottom part) of an optical pulse. It begins with a Fourier-limited, ultrafast optical pulse, which is chirped in a highly dispersive chirped fibre Bragg grating (CFBG), increasing its duration from single picoseconds to single nanoseconds. Such chirp linearly separates different spectral components of the optical pulse in time due to applied quadratic spectral phase $\phi(\omega)$. Then time-dependent spectral shear is applied in the form of quadratic modulo 2π temporal phase, shifting all the spectral components towards the central wavelength, hence performing a spectral compression. By using phase periodicity of 2π one achieves ns-long temporal waveforms, resulting in compression of the spectral width of optical pulses by many orders of magnitude, to sub-GHz widths.

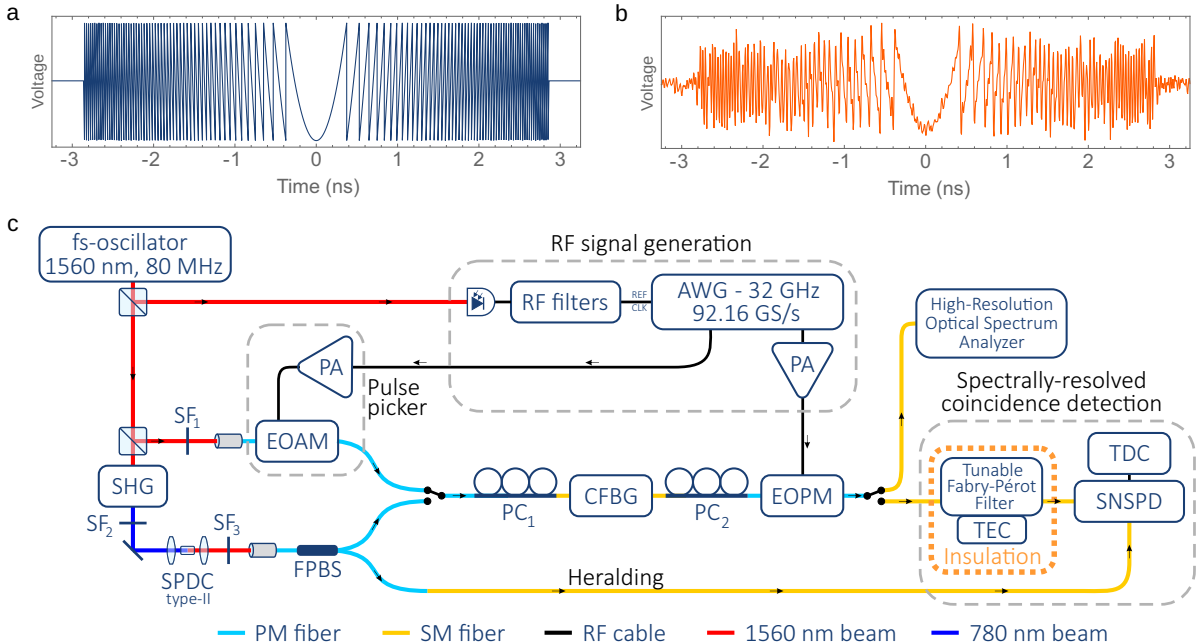


Figure 2. **Experimental setup and Fresnel waveforms.** **a** The ideal Fresnel waveform. **b** A measured oscilloscope (63 GHz electronic bandwidth) trace of the generated Fresnel waveform, corresponding to 10 ns/nm of dispersion. It was precompensated (see Methods), transmitted through the whole RF system and measured at the RF output of the EOPM. **c** Schematic of the experimental setup. The optical pulses originating in an Er-doped femtosecond oscillator and amplifier are divided into three paths by a set of beamsplitters. In the first one, they are directly detected via a photodiode followed by a set of RF filters to generate a clock signal for radio-frequency (RF) system synchronization. In the second path, optical pulses are spectrally shaped (SF_1) and passed through a home-built pulse picker using an electro-optic amplitude modulator (EOAM) to decrease the repetition rate. Then they are chirped in a chirped fibre Bragg grating (CFBG) placed between two polarization controllers ($PC_{1,2}$), spectrally compressed in an electro-optic phase modulator (EOPM) driven by an amplified (PA) RF signal from an arbitrary waveform generator (AWG) and measured by a high-resolution optical spectrum analyser. Single-photon measurements utilise the third path, where optical pulses are frequency-doubled to generate photon pairs in a type-II spontaneous parametric down-conversion (SPDC) process. The photon pairs are split in a fibre polarization beamsplitter (FPBS), where one of them – the herald – is sent directly to a superconducting nanowire single-photon detector (SNSPD) and time-tagged (TDC) for coincidence counting. The signal photon undergoes the same spectral compression as the classical optical pulses but is detected by another SNSPD after passing through a high-finesse Fabry-Pérot filter. The filter is swept by a piezo element driven by a programmable power supply to retrieve information on the single-photon spectra. Additionally, the filter emulates a narrowband absorber, such as an atomic system.

tion amplitude [29, 30].

Here we show a phase-only quantum interface bridging the ultrafast and slow classes of QI-processing system. We overcome the limit of electro-optic modulation amplitude by exploiting the phase periodicity, in analogy to a Fresnel lens [31]. We replace a standard parabolic electro-optic waveform with a complex phase-wrapped one. By combining it with off-the-shelf low-loss dispersive elements and advanced wide-bandwidth electronics, we demonstrate a quantum interface able to efficiently compress single-photon spectral bandwidth by many orders of magnitude, from picosecond to nanosecond timescales [32].

Spectral bandwidth compression requires manipulation of both the temporal envelope and spectrum of an optical pulse. It consists of two stages, see Fig. 1. First, a spectrally wide-band optical pulse is chirped in a dispersive medium. It increases the duration of the pulse, while simultaneously linearly separating its different spectral components in time. Chirping corresponds to application of a quadratic spectral phase $\phi(\omega) = \Phi\omega^2/2$, where Φ is the group delay dispersion (GDD) and ω is the angular frequency. Subsequently, a time-dependent spectral shear is applied to the pulse such that all spectral components are shifted towards a single central wavelength, reshaping the spectrum into a narrower one. It is achieved by applying quadratic temporal phase $\varphi(t) = Kt^2/2$, where K is the chirping factor and t is the retarded time. It can be also viewed as a spectral shift changing linearly in time [33]. When the condition $K = \Phi^{-1}$ is met, different spectral components are shifted directly towards the centre of the pulse spectrum. One obtains it by modulating the optical pulses via electro-optic phase modulation driven by a voltage signal quadratic in time. Such an operation is called a time lens due to its mathematical analogy to a quadratic spatial phase introduced by a regular lens [29, 30].

Chirping single-picosecond pulses to nanosecond duration requires a highly-dispersive medium with the lowest possible loss. For this reason, we use chirped fibre Bragg gratings (CFBG) with dispersion of 5 ns/nm or 10 ns/nm, commercially available at telecom wavelengths with insertion losses below 3 dB.

The duration of the quadratic temporal phase has to match the output nanosecond optical pulse duration. The standard approach of using a single-tone RF (sine) signal driving an electro-optic phase modulator (EOPM) limits the achievable compression factor. This is because of low modulation frequency, required to cover the whole nanosecond long output optical pulse. Combined with the limit on maximal phase modulation amplitude, due to the breakdown voltage of the electro-optic modulator, it limits the achievable spectral shifts, yielding a low compression factor [23, 28–30]. Here we overcome this challenge by using a modulation scheme with a complex temporal phase, taking advantage of the phase periodicity [32], i.e. using a quadratic temporal phase modulo 2π factor. Such an approach, inspired by the spatial Fresnel lens [31], allows achieving a very long parabolic phase with steep slopes while limiting the necessary modulation amplitude to just 2π , which is accessible for commercially available EOPMs.

Generation of Fresnel-like waveforms requires using advanced wide-bandwidth RF electronics. In particular, one needs a high-speed arbitrary waveform generator due to the waveform complexity. In contrast to the standard electro-optic time lens, where a single frequency signal is used, a Fresnel waveform contains a wide range of frequencies, with the

highest frequency components originating from the wrapping points, see Fig. 2a. Additionally, the instantaneous frequency of a quadratic function – its slope – is increasing linearly in both directions from the waveform’s centre, with its maximal value limited by the RF system’s electronic bandwidth f_{BW} . It induces a limitation on the waveform duration and on the

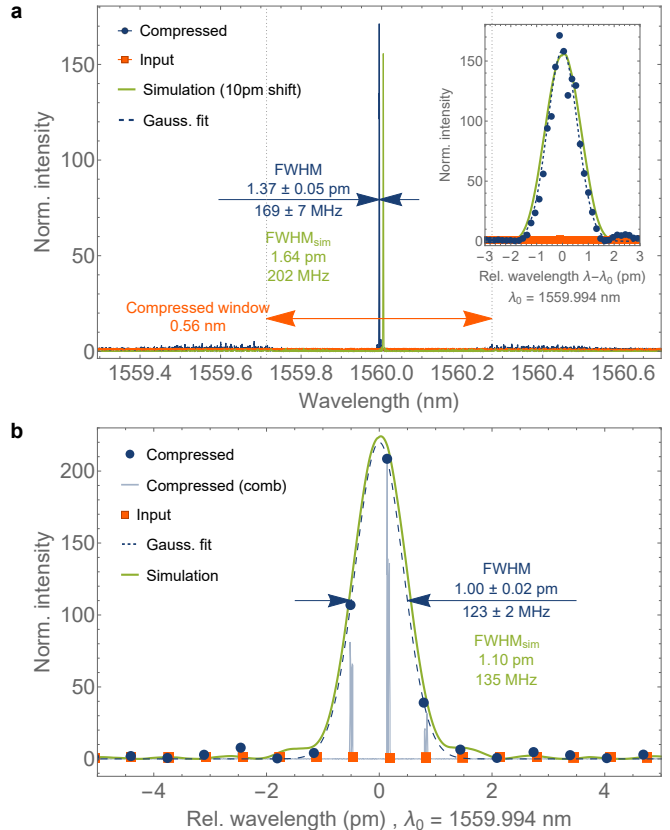


Figure 3. Spectral compression of coherent laser pulses. **a** Spectra of input (orange), compressed (blue) and simulated (green) coherent laser pulses using a 10 ns/nm dispersion module, normalized to the maximum of the input spectrum. The inset shows the same spectrum in the narrower range of 6 pm, where each point originates from an individual longitudinal mode (see Methods), which samples the spectral envelope. To increase the number of measurement points the laser light was pulsed-picked to reduce the repetition rate to 20 MHz, hence increase the density of longitudinal modes. The spectral compression factor of 408 and maximal spectral intensity enhancement by a factor of 154 yields compression efficiency of 40.6% [32]. The plot does not include the 31.9% transmission of the setup due to technical losses. **b** Increasing the dispersion to 15 ns/nm yields even higher enhancement of the maximal intensity. Here we disabled the pulse-picking, resulting in generation of a quasi-continuous wave (CW) light, with compressed pulse duration approaching the pulse repetition rate. The light blue line shows the raw measured spectrum, with distinct longitudinal modes of the optical pulses. Due to width of the spectral envelope close to the repetition rate, which is equal to the longitudinal modes separation, only a single longitudinal mode dominates, confirming the quasi-CW regime.

maximal achievable spectral shift at the edges of the waveform [33]. As a consequence, it restricts the maximal spectral width of the input optical pulses to $\Delta f = 2f_{\text{BW}}$. Our selection of RF equipment with about 35 GHz RF bandwidth limits the maximal spectral shift to 35 GHz, which yields a 0.56 nm (70 GHz) wide spectral input window at telecom wavelengths. The non-flat frequency responses of all the RF electronics introduce distortions of the generated waveform. We used frequency response precompensation (see Methods) to counteract them. An exemplary oscilloscope (63 GHz electronic bandwidth) trace is shown in Fig. 2b, measured at the output of the whole RF system, shown in Fig. 2c.

First, we directly show the spectral compression employing classical light pulses using the setup shown schematically in Fig 2c. The optical pulses from the erbium-doped fibre oscillator and amplifier were spectrally filtered (SF_1), pulse-picked, and then chirped in a CFBG module. Then a temporal phase in the form of a Fresnel waveform was applied in the EOPM. Finally, the laser pulses were detected with a high-resolution (5 MHz) optical spectrum analyser. The applied phase waveforms were generated with the AWG and synchronized to the optical pulses by its internal phase-lock loop (PLL), see Methods.

In Fig. 3a, we show input and compressed spectra when a chirping module with a dispersion of 10 ns/nm and a 20 MHz pulse repetition rate was used. The inset shows the same spectrum within a narrower wavelength range, where each point originates from an individual longitudinal mode of the laser, see Methods. The spectra are normalized to the maximal intensity of the input spectrum. Both spectra are measured at the output of the whole system, whose power transmission was 31.9%. We show 154-fold (without losses), or 49-fold (including losses) enhanced maximal intensity, with full width at half maximum (FWHM) of 1.37 ± 0.03 pm (168 ± 7 MHz), measured by fitting a Gaussian profile to the compressed spectral peak. It yields an efficiency of 40.6%, measured as a fraction of the light intensity within the compressed peak. The non-unit value of efficiency results from the nonidealities of the generated Fresnel waveform, which cause shifting some spectral components in the wrong direction – these can be observed as low spectral peaks outside of the compressed window in Fig. 3a. The measured spectra show good agreement with simulations (see Methods) shown with a green line.

Next, we increased the dispersion to 15 ns/nm by joining two CFBG modules (5 ns/nm and 10 ns/nm). Additionally, we increased the repetition rate to 80 MHz, by disabling the pulse picker. By using an appropriately modified Fresnel waveform, we obtained an even higher enhancement of over 220 (without loss) and an efficiency of 38.7%, shown in Fig. 3b. However, due to the use of two separate CFBG modules, introducing in total more loss of 16%, including the EOPM, the enhancement with system transmission taken into account was 35.2. Here we also show the generation of quasi-CW light. The FWHM of the compressed spectra is 1.00 ± 0.02 pm (123 ± 2 MHz), which is very close to the repetition rate of 80 MHz. It means that one longitudinal mode dominates under the spectral envelope, as shown in Fig. 3b, where the blue, dashed line shows fitted Gaussian envelope and raw measured spectrum, with clearly visible laser longitudinal modes (comb), is shown by the light blue line (see Methods).

To confirm the contribution of the phase-wrapped part of the Fresnel waveform on the spectral compression, we measured the enhancement when artificially limiting the dura-

tion of the waveform. Because the instantaneous frequency of the signal, proportional to its slope, increases linearly for the quadratic function, we limited the waveform up to the point where it meets the cut-off frequency f_{max} , which we changed in the range of 5 to 52 GHz, see Fig. 4. We show a nearly linearly increasing enhancement with the cut-off frequency up to the bandwidth of the RF system of 35 GHz, after which we reach a plateau. It clearly shows that the Fresnel-like waveforms take advantage of the whole available RF bandwidth.

To directly verify our approach to large-scale spectral compression of quantum light pulses for applications in quantum networks, we prepared pure single photons via heralded spontaneous parametric down-conversion process [4] pumped with frequency-doubled laser pulses originating from the same laser as above, see Fig. 2c (see Methods). Then the single photons were propagated through the same 10 ns/nm CFBG and EOPM as for the case of classical light. Finally, they were detected with a superconducting nanowire single-photon detector (SNSPD) after passing through a high-finesse tunable Fabry-Pérot interference filter with 420 MHz FWHM spectral bandwidth (see Methods), simulating a narrowband absorber like an atomic system. Then coincidences of signal and idler photons are found with a time-to-digital converter (TDC). In Fig. 5 we show the measured 51-fold increased heralded single-photon flux of the compressed single-photon spectra (blue) in comparison to the input (orange) in the case of a lossless system. Taking into account the technical transmission of the CFBG and EOPM of 31.9% results with the overall enhancement of a 16. It proves that such a system can be used to enhance the absorption or interference rates of bandwidth-incompatible photon pulses. The 16-fold enhance-

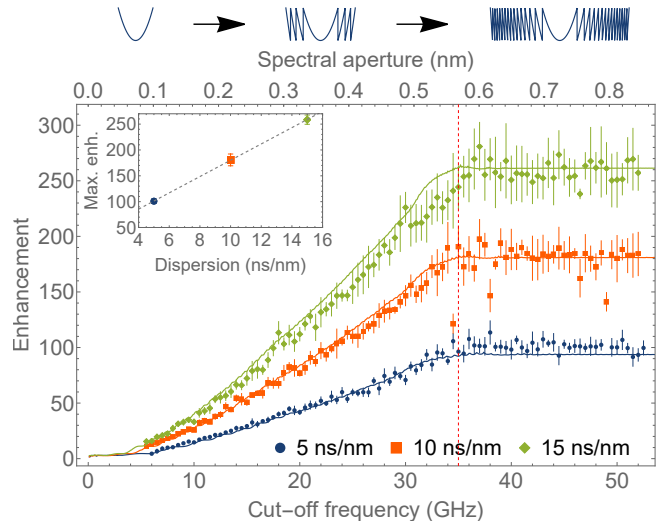


Figure 4. Fresnel time lens aperture By artificially limiting the Fresnel-waveform duration, i.e. the time lens aperture, as shown in the top panel, we measure the lossless enhancement for three different dispersions of 5 (blue), 10 (orange) and 15 ns/nm (green). The limitation is given by the maximal instantaneous frequency of the parabola, which also yields maximal spectral shift. The enhancement increases linearly up to the RF bandwidth f_{BW} , shown with a red dashed line. The inset shows the maximal enhancement in function of used group delay dispersion (GDD). Solid lines show simulation results for each value of dispersion.

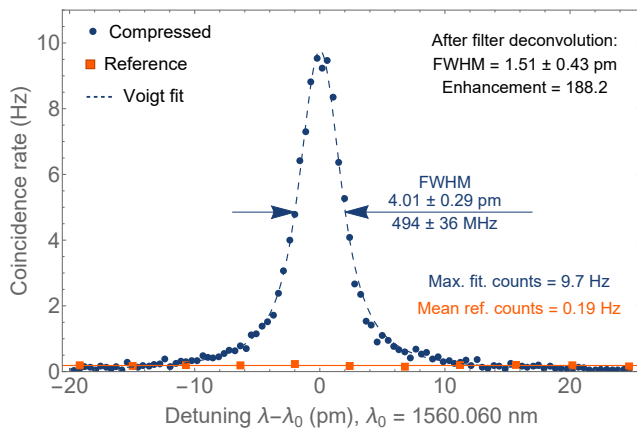


Figure 5. **Spectral manipulation of single-photon wavepackets.** Coincidence counts of photons passing through a narrowband filter with compression (blue dots) and without compression (orange squares). To avoid introducing arbitrary parameters the reference signal was measured for photons going through the same setup, but without applying temporal phase (see Methods), while the transmission of 31.9% of the setup was measured separately. The coincidence rate was measured for 1 min/bin for compressed and 5 min/bin for reference signal. The filter was detuned to measure spectral shape of the spectrum with the results fitted with Voigt profile (see text).

ment would be further improved using a spectrally narrower absorber; here, the absorption line was larger than the single-photon spectral width limiting the obtained enhancement.

To find the upper bound of the enhancement for an absorber with linewidth much smaller than single-photon spectral width, we measured the single-photon spectral shape by detuning the Fabry-Pérot interference filter. It was then fitted with the Voigt profile, shown by the blue dashed line in Fig. 5. Such a profile is a convolution of the single-photon spectrum’s Gaussian shape and the interference filter’s Lorentzian shape with a fixed width measured independently. Deconvolving the Gaussian width from the fit yields a single-photon spec-

tral width of 1.51 ± 0.43 pm (186 ± 53 MHz) and enhancement (without technical losses) of 188.2, which agrees well with the results for classical light shown in Fig 3a. Including the 31.9% transmission of the system, we expect the enhancement of absorbed single photon flux by a factor of up to 60 for absorber’s linewidths smaller than compressed single-photon spectral width.

We demonstrate that complex electro-optic temporal phase modulation enables spectral compression of classical and quantum light pulses by over 2 orders of magnitude, from tens of GHz to hundreds of MHz, reaching the regime of matter-based quantum information processing platforms. To this end we developed a Fresnel time lens, which takes the advantage of phase periodicity and all of the available RF system bandwidth. We applied this method to reduce spectral bandwidths of heralded single photons down to single pm, while enhancing their maximal spectral intensity. By simulating a narrowband absorber with a narrowband filter we measured a 16-fold increase of photon flux through the filter as compared to direct connection. We expect to further increase this value up to 60 for absorbers with spectral linewidths narrower than the compressed pulse spectrum. Such a low-loss, all-fibre and easily reconfigurable electro-optic quantum interface will allow to increase absorption and/or multi-photon interference rates in the future hybrid quantum networks, where both ultrafast and atomic-based systems will be employed. Not only it will enable efficient network operation, but may facilitate efficient establishing of long-distance entanglement between quantum network nodes.

Development of high-speed RF devices with commercially available bandwidths of 70 GHz, as well as lower loss chirped fibre Bragg gratings will allow to further boost the performance of such an electro-optic quantum interface. Moreover, our device shows high potential to be used in an on-chip configuration, where bandwidths over 100 GHz with low V_π have been reported in the thin-film lithium niobate platform [34, 35]. Finally, employing a complex temporal phase modulation is a significant step towards arbitrary shaping of quantum light in the spectro-temporal degree of freedom [36–38].

-
- [1] Gisin, N. & Thew, R. Quantum communication. *Nature Photonics* **1**, 165–171 (2007).
 - [2] Simon, C. Towards a global quantum network. *Nature Photonics* **11**, 678–680 (2017).
 - [3] Weiner, A. M. Ultrafast optical pulse shaping: A tutorial review. *Optics Communications* **284**, 3669–3692 (2011).
 - [4] Mosley, P. J. *et al.* Heralded generation of ultrafast single photons in pure quantum states. *Physical Review Letters* **100**, 133601 (2008).
 - [5] MacLean, J.-P. W., Donohue, J. M. & Resch, K. J. Direct characterization of ultrafast energy-time entangled photon pairs. *Physical Review Letters* **120**, 053601 (2018).
 - [6] Saffman, M., Walker, T. G. & Mølmer, K. Quantum information with rydberg atoms. *Reviews of Modern Physics* **82**, 2313 (2010).
 - [7] Reiserer, A., Kalb, N., Rempe, G. & Ritter, S. A quantum gate between a flying optical photon and a single trapped atom. *Nature* **508**, 237–240 (2014).
 - [8] Lvovsky, A. I., Sanders, B. C. & Tittel, W. Optical quantum memory. *Nature Photonics* **3** (2009).
 - [9] Jensen, K. *et al.* Quantum memory for entangled continuous-variable states. *Nature Physics* **7**, 13–16 (2011).
 - [10] Blatt, R. & Roos, C. F. Quantum simulations with trapped ions. *Nature Physics* **8**, 277–284 (2012).
 - [11] Aharonovich, I., Englund, D. & Toth, M. Solid-state single-photon emitters. *Nature Photonics* **10**, 631–641 (2016).
 - [12] Lago-Rivera, D., Grandi, S., Rakonjac, J. V., Seri, A. & de Riedmatten, H. Telecom-heralded entanglement between multimode solid-state quantum memories. *Nature* **594** (2021).
 - [13] Wallucks, A., Marinković, I., Hensen, B., Stockill, R. & Gröblacher, S. A quantum memory at telecom wave-

- lengths. *Nature Physics* **16**, 772–777 (2020).
- [14] Duan, L. M., Lukin, M. D., Cirac, J. I. & Zoller, P. Long-distance quantum communication with atomic ensembles and linear optics. *Nature* **414**, 413–418 (2001).
- [15] Wang, Y. *et al.* Single-qubit quantum memory exceeding ten-minute coherence-time. *Nature Photonics* **11**, 646–650 (2017).
- [16] Kaczmarek, K. T. *et al.* High-speed noise-free optical quantum memory. *Physical Review A* **97**, 042316 (2018).
- [17] Fushman, I. *et al.* Controlled phase shifts with a single quantum dot. *Science* **320**, 769–772 (2008).
- [18] Tiarks, D., Schmidt, S., Rempe, G. & Dür, S. Optical π phase shift created with single-photon pulse. *Science Advances* **2**, e160003 (2016).
- [19] Kimble, H. J. The quantum internet. *Nature* **453**, 1023–1030 (2008).
- [20] Wehner, S., Elkouss, D. & Hanson, R. Quantum internet: A vision for the road ahead. *Science* **362**, eaam9288 (2018).
- [21] Ou, Z. Y. & Lu, Y. J. Cavity enhanced spontaneous parametric down-conversion for the prolongation of correlation time between conjugate photons. *Physical Review Letters* **83**, 2556 (1999).
- [22] Lavoie, J., Donohue, J. M., Wright, L. G., Fedrizzi, A. & Resch, K. J. Spectral compression of single photons. *Nature Photonics* **7**, 363–366 (2013).
- [23] Karpiński, M., Jachura, M., Wright, L. J. & Smith, B. J. Bandwidth manipulation of quantum light by an electro-optic time lens. *Nature Photonics* **11**, 53–57 (2017).
- [24] Agha, I., Ates, S., Sapienza, L. & Srinivasan, K. Spectral broadening and shaping of nanosecond pulses: toward shaping of single photons from quantum emitters. *Optics Letters* **39**, 5677–5680 (2014).
- [25] Matsuda, N. Deterministic reshaping of single-photon spectra using cross-phase modulation. *Science advances* **2**, e1501223 (2016).
- [26] Salem, R. *et al.* Optical time lens based on four-wave mixing on a silicon chip. *Optics Letters* **33**, 1047–1049 (2008).
- [27] Joshi, C. *et al.* Picosecond-resolution single-photon time lens for temporal mode quantum processing. *Optica* **9**, 364–373 (2022).
- [28] Sośnicki, F., Mikołajczyk, M., Golestani, A. & Karpiński, M. Aperiodic electro-optic time lens for spectral manipulation of single-photon pulses. *Applied Physics Letters* **116**, 234003 (2020).
- [29] Kolner, B. H. Space-time duality and the theory of temporal imaging. *IEEE Journal of Quantum Electronics* **30**, 1951–1963 (1994).
- [30] Torres-Company, V., Lancis, J. & Andres, P. Space-time analogies in optics. *Progress in Optics* **56**, 1–80 (2011).
- [31] Fresnel, A. *Mémoire sur un nouveau système d'éclairage des phares* (Imprimerie royale, Paris, 1822).
- [32] Sośnicki, F. & Karpiński, M. Large-scale spectral bandwidth compression by complex electro-optic temporal phase modulation. *Optics Express* **26**, 31307–31316 (2018).
- [33] Wright, L. J., Karpiński, M., Söller, C. & Smith, B. J. Spectral shearing of quantum light pulses by electro-optic phase modulation. *Physical Review Letters* **118**, 023601 (2017).
- [34] Wang, C. *et al.* Integrated lithium niobate electro-optic modulators operating at cmos-compatible voltages. *Nature* **562**, 101–104 (2018).
- [35] Zhu, D. *et al.* Spectral control of nonclassical light using an integrated thin-film lithium niobate modulator. *arXiv:2112.09961* .
- [36] Kielpinski, D., F., C. J. & Wiseman, H. M. Quantum optical waveform conversion. *Physical Review Letters* **106**, 130501 (2011).
- [37] Ashby, J. *et al.* Temporal mode transformations by sequential time and frequency phase modulation for applications in quantum information science. *Optics Express* **28**, 38376–38389 (2020).
- [38] Karpiński, M., Davis, A. O. C., Sośnicki, F., Thiel, V. & Smith, B. J. Control and measurement of quantum light pulses for quantum information science and technology. *Advanced Quantum Technologies* **4**, 2000150 (2021).

Methods

RF waveform generation

The waveforms have been calculated according to the parameters: K – chirping rate of the time lens, spectral aperture δf (see Main text), and $SR = 92.16$ GS/s being a sampling rate of the arbitrary waveform generator (AWG). The duration of the whole waveform was limited to $\Delta t = 2\delta t = 4\pi\delta f/K$. The waveforms were then divided by the complex frequency response of the RF system (measured separately) in the frequency domain within the range of RF bandwidth of the system. The resulting waveform in the time domain was generated in the AWG (Keysight M8196A, 35 GHz RF bandwidth), amplified with a high-bandwidth power amplifier (RFLambda, 0.2 – 35 GHz, 2 W). It was driving an electro-optic phase modulator (EOSpace, $V_{\pi@1\text{ GHz}} = 3\text{ V}$, 2.4 dB insertion loss). Every change of the waveform parameters changes its minimal and maximal value. Therefore to find the peak-to-peak amplitude of the waveform corresponding to the 2π peak-to-peak amplitude of the phase the RF amplitude was swept to find maximal spectral compression.

Classical spectrum measurements

Spectra of classical, coherent light were acquired with a high-resolution optical spectrum analyser (APEX A2681, 5 MHz resolution). Since this resolution is higher than the repetition rate of 80 MHz or 20 MHz, individual longitudinal modes were found and summed over, creating a spectral envelope sampled with resolution given by the repetition rate. The home-built pulse picker was used to reduce the repetition rate and hence increase the resolution of measured spectra. The pulse-picker was built by utilizing a second channel of the AWG, generating rectangular pulses, which were amplified (Keysight N4985a-S50) and were driving an electro-optic amplitude modulator (Thorlabs LN05S-FC).

Some of heralded single photons

Laser pulses originating from an erbium-doped fibre oscillator (Menlo C-Fiber 780HP) with repetition rate of 80 MHz and central wavelength 1560 nm are frequency doubled (Menlo C-Fiber 780HP) yielding a second harmonic beam with central wavelength of 780 nm. This pump beam passes through a $4f$ tunable spectral filter and is then focused into a 10 mm long periodically-poled potassium titanyl phosphate (PPKTP) crystal, where type-II spontaneous parametric down-conversion (SPDC) takes place creating, orthogonally polarized photon pairs. The pump beam is spectrally filtered such that produced photon pairs are wavelength-degenerate and spectrally uncorrelated. The photon pair beam is recollimated and additionally spectrally filtered with a set of interference filters to 1 nm FWHM such that the whole spectrum could be measured with sweeping the Fabry-Pérot interference filter with free spectral range (FSR)

of 1.2 nm. Then the photon pairs are coupled into a polarization maintaining (PM) fibre and photons from each pair – signal and idler – are separated by a fibre polarisation beamsplitter (FPBS). The idler photon is sent directly to a superconducting nanowire single-photon detector (SingleQuantum) heralding the signal photon. A time-to-digital converter (TDC, Swabian TimeTagger Ultra) is used to register coincidence events of detecting heralding idler photons and heralded signal photons.

Spectrally narrowband absorber . The narrowband absorber was realized with a fibre-pigtailed high-finesse tunable Fabry-Pérot interference filter (Micron Optics FFP-TF2) with 420 MHz FWHM passband and 1.2 nm measured FSR. The tuning of the filter was automated with a stable programmable power supply (Keysight E36313A) driving a piezo-element within the filter. To thermal isolation and precise temperature control allowed to reduce the thermal drifts to below 1 pm within the measurement time. Because of a very low count rate through the filter, due to its narrowband transmission, i.e. filtering most of the photons, the coincidence count rates shown in Fig. 5 were measured without disconnecting the CFBG and EOPM. This was to avoid introducing any arbitrary parameters such as additional polarisation mismatch from fibres reconnections or thermal drift, which could not be realigned due to the low count rate. Therefore the transmission of the setup was measured separately.

Simulations . The simulations were based on ref. [32]. Their inputs are waveforms sent to the AWG and measured input (reference) spectrum. Then the waveform is discretized in time according to the sample rate and in amplitude according to the effective number of bits (ENOB) of the AWG. Then a set of a complex frequency responses of the elements is applied by multiplication. By series of applying temporal or spectral phase and fast Fourier transforms (FFT) a quadratic spectral phase and the simulated temporal phase waveform are applied to the input spectra yielding an output spectra, shown as a green line in Fig. 3 and its enhance-

ment shown by solid lines in Fig.4. The simulations do not take into account a time-interval error (jitter).

Author contributions

M.K. conceived and supervised the project. F.S. designed and performed the experiment with an input from M.M., who build a photon-pair source and tunable spectral filter. A. G. contributed to the early stages of the experiment. F.S and M.K. wrote the manuscript. F.S. prepared the figures.

Acknowledgements

We thank B. J. Smith, M. Jachura, and A. Widomski for insightful comments and discussions. We thank Keysight and AM Technologies for equipment loan. The research was funded in parts by the First TEAM (Project No. POIR.04.04.00-00-5E00/18) and HOMING (Project No. POIR.04.04.00-00-5E00/18) programmes of the Foundation for Polish Science, co-financed by the European Union under the European Regional Development, and in part by the National Science Centre of Poland (Project No. 2019/32/Z/ST2/00018, QuantERA project QuICHE).

Competing Interests

The authors declare that they have no competing financial interests.

Correspondence

Correspondence and requests for materials should be addressed to F.S. (e-mail: Filip.Sosnicki@fuw.edu.pl).